Satellite observed changes in the Northern Hemisphere snow cover phenology and the associated radiative forcing and feedback between 1982 and 2013

2016 Environ. Res. Lett. 11 084002

(http://iopscience.iop.org/1748-9326/11/8/084002)

Environmental Research Letters

LETTER

Satellite observed changes in the Northern Hemisphere snow cover phenology and the associated radiative forcing and feedback between 1982 and 2013

Xiaona Chen[1,2,3], **Shunlin Liang**[1,2] **and Yunfeng Cao**[1,2]

[1] State Key Laboratory of Remote Sensing Science, School of Geography, Beijing Normal University, Beijing 100875, People's Republic of China
[2] Department of Geographical Sciences, University of Maryland, College Park 20740, USA
[3] State Key Laboratory of Hydroscience and Engineering, Department of Hydraulic Engineering, Tsinghua University, Beijing 100084, People's Republic of China

E-mail: sliang@bnu.edu.cn

Keywords: snow cover phenology, climate change, global warming, Northern Hemisphere

Supplementary material for this article is available online

OPEN ACCESS

RECEIVED
26 February 2016

REVISED
5 July 2016

ACCEPTED FOR PUBLICATION
19 July 2016

PUBLISHED
28 July 2016

Abstract

Quantifying continental-scale changes in snow cover phenology (SCP) and evaluating their associated radiative forcing and feedback is essential for meteorological, hydrological, ecological, and societal purposes. However, the current SCP research is inadequate because few published studies have explored the long-term changes in SCP, as well as their associated radiative forcing and feedback in the context of global warming. Based on satellite-observed snow cover extent (SCE) and land surface albedo datasets, and using a radiative kernel modeling method, this study quantified changes in SCP and the associated radiative forcing and feedback over the Northern Hemisphere (NH) snow-covered landmass from 1982 to 2013. The monthly SCE anomaly over the NH displayed a significant decreasing trend from May to August (-0.89×10^6 km^2 decade^{-1}), while an increasing trend from November to February (0.65×10^6 km^2 decade^{-1}) over that period. The changes in SCE resulted in corresponding anomalies in SCP. The snow onset date (D_o) moved forward slightly, but the snow end date (D_e) advanced significantly at the rate of 1.91 days decade^{-1}, with a 73% contribution from decreased SCE in Eurasia (EU). The anomalies in D_e resulted in a weakened snow radiative forcing of 0.12 ($\pm$0.003) W m^{-2} and feedback of 0.21 ($\pm$0.005) W m^{-2} K^{-1}, in melting season, over the NH, from 1982 to 2013. Compared with the SCP changes in EU, the SCP anomalies in North America were relatively stable because of the clearly contrasting D_e anomalies between the mid- and high latitudes in this region.

1. Introduction

The snow cover extent (SCE) and snow cover phenology (SCP) over the Northern Hemisphere (NH) play a crucial role in the Earth's hydrology and surface energy balance, and modulate the feedbacks that control variations in global climate (Frei *et al* 2012, Peng *et al* 2013, Brands 2014, Chen *et al* 2015). The Eurasian snow cover in October is closely related with the December–February mean boreal winter climate via the 10 m wind speed and significant wave heights in the North Atlantic and adjacent seas (Brands 2014). Changes in the Eurasian fall snow cover could be a potential driver of changes in the Arctic Oscillation. Such changes may also provide a link between the decline in sea-ice in the Arctic during summer and the unusual atmospheric circulation the following winter (Wegmann *et al* 2015). Trends in the duration or extent of the snow cover are expected to exert feedback on the temperature trends (Peng *et al* 2013). In a warmer climate, snow will melt earlier in the year; and this has already been occurring in some places (Barnett *et al* 2005). Moreover, snow cover changes are also likely to impact the carbon pool stored in the

permafrost (Gouttevin *et al* 2012). SCP is highly correlated with various biological phenomena that depend on the accumulated temperature, such as animal migrations and vegetation growth (Bokhorst *et al* 2009). In addition, the surface radiative and turbulent fluxes in spring and summer have strong correlations with satellite-observed SCE (Barnett *et al* 2005). Changes in the snow cover in the NH landmasses enhance climatic anomalies through radiative forcing and snow-albedo feedback (SAF) effects. As surface air temperature increases, the snow cover over the NH extra-tropical region retreats, which causes the land surface to reflect less solar radiation. The extra radiation is absorbed, resulting in enhanced warming, especially in the regions undergoing snow and ice reduction (Hall 2004). This SAF accounts for approximately half of the additional net incoming solar radiation associated with the retreat of the NH cryosphere in equilibrium climate change simulations (Hall 2004, Qu and Hall 2006). Thus, monitoring the SCE and SCP is essential to assess the impacts of climate change and projections of future climate, especially in the snow-dominated regions.

Previous studies have proven that SCE in the NH has experienced a well-documented rapid decrease since satellite observations began in the late 1960 s. Climate projections suggest that the SCE will continue shrinking in the future (Brown and Robinson 2011, IPCC 2013), coinciding with the hemispheric warming and indicating the positive feedback of surface reflectivity on climate (e.g. Brown *et al* 2010, Brown and Robinson 2011, Flanner *et al* 2011). In response to the variability of SCE, the SCP has also experienced remarkable changes. Such changes include the shortening of snow cover duration days (D_d) (e.g. Whetton *et al* 1996, Choi *et al* 2010), with an earlier snow melt onset (Wang *et al* 2013), an advanced snow end date (D_e), and a delayed snow onset date (D_o) (Choi *et al* 2010), at both the local and regional scales. However, only a few of these studies have explored the effects of long-term SCP changes on the radiative forcing and its associated feedback. The effects of long-term SCP changes on the Earth's climate system and energy budget are still unclear. Additionally, most published studies are based on *in situ* observations or models in which the *in situ* measurements are highly dependent on a particular location (latitude and elevation), hence limiting the model outputs with assumptions. Moreover, published estimates of SCP focus mainly on high-latitude regions of the NH, and conditions at the hemispheric scale are rarely documented.

Given the importance of SCP in the Earth's climate system and in the current climate change background, it is necessary to quantify and understand its spatial and temporal anomalies, and to clarify its associated radiative forcing and feedback onto the Earth's climate system, using long-term satellite observations. Therefore, the objective of this study is to quantify long-term changes in SCP based on satellite observations and to explore its associated snow radiative forcing (S_nRF) and albedo feedback over the NH snow-covered landmass between 1982 and 2013. In order to achieve this objective, we first quantified the SCE anomalies over the NH. Then, we retrieved the D_o, D_e, and D_d based on the observed changes in SCE. Finally, we calculated the associated S_nRF and albedo feedback using the radiative kernel technology.

2. Data and methods

2.1. Datasets

To investigate the latest SCE changes over the NH, we employed the widely used monthly SCE chart data generated by the Rutgers University Global Snow Lab and the binary snow cover mask data derived from the Climate Data Record of Northern Hemisphere Snow Cover Extent (NHSCE) at a spatial resolution of 25 km in this study. Both the chart data and the binary snow cover mask data were developed by Robinson *et al* (1993).

The NHSCE data was derived from manual interpretation of Advanced Very High Resolution Radiometer (AVHRR), Geostationary Operational Environmental Satellite, and other visible-band satellite data (Helfrich *et al* 2007). An uncertainty analysis for NHSCE in March and April was conducted, estimated from an inter-comparison of multiple datasets by Brown and Robinson (2011). It indicated a 95% confidence level in SCE estimations of ±3–5% over the satellite era begun in the late 1960 s. Since the binary value in the NHSCE dataset indicates a 50% or larger probability of occurrence of snow in each pixel, this data is more appropriate for large-scale snow cover studies. However, this dataset is still valuable in large-scale snow related studies. For instance, Choi *et al* (2010) derived the information on snow seasons from NHSCE and found that the duration of the average NH full snow season has decreased significantly between the winters of 1972/73 and 2007/08; Derksen and Brown (2012) estimated the spring SCE over the NH using NHSCE between 1967 and 2012, compared it with the Coupled Model Inter-comparison Project Phase 5 (CMIP5) model output, and concluded that the reductions of the spring SCE in the 2008–2012 period exceeded the CMIP5 projections.

To calculate the albedo contrast (Δa_s) induced by changes in SCP, we employed the newly released long-term, high-quality, and spatially complete Global LAnd Surface Satellite (GLASS) land surface albedo (a_s) product (Liang *et al* 2013) in 0.05° spatial resolution over the 1982–2013 period, and the MODerate resolution Imaging Spectroradiometer (MODIS)-derived global gap-filled and snow-free a_s product (MCD43GF) (Moody *et al* 2008) in about 0.0083° spatial resolution between 2001 and 2013. The GLASS a_s is a real time series of surface albedos and the MCD43GF a_s is a snow-free albedo. We then obtained

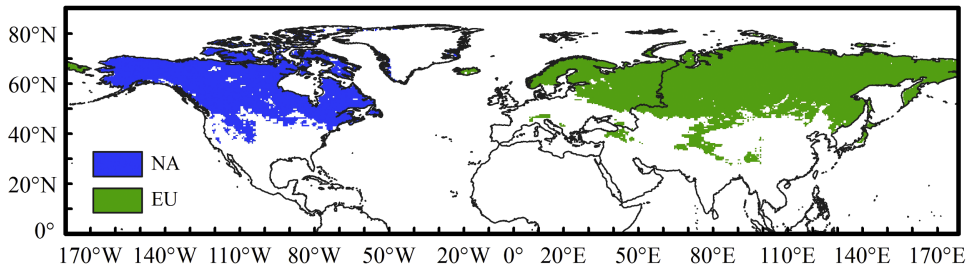

Figure 1. Study area over the Northern Hemisphere, including North America (NA) and Eurasia (EU).

in the present study the Δa_s time series (yearly and monthly) from the GLASS a_s, minus the climatology snow-free a_s obtained from MCD43GF. The GLASS a_s dataset was produced from both AVHRR and MODIS data (Liang *et al* 2013) and has previously been used to quantify the radiative forcing of snow melt over Greenland (He *et al* 2013) and snow cover changes over China (Chen *et al* 2016), with high quality and fine spatial resolution. The spatially complete MCD43GF snow-free a_s was produced using an ecosystem-reliant temporal interpolation technique that retrieves missing data with an error of 3%–8% (Moody *et al* 2008).

In order to quantify the S_nRF and the feedback caused by a_s changes induced by SCP anomalies, the albedo radiative kernel expressed as the net shortwave (SW) anomalies at the top of the atmosphere (TOA) and associated with a 1% change in the a_s was used. Such data was estimated using radiative transfer codes from the Community Atmosphere Model (CAM3) of the National Center for Atmosphere Research and the Atmosphere Model 2 (AM2) of the Geographical Fluid Dynamic Laboratory developed by Shell *et al* (2008) and Soden *et al* (2008).

2.2. Methods

2.2.1. SCP retrieval

To discern variations in the NH SCP, the snow cover region (grid cells) was defined as the area between 30° N and 75°N, excluding grid cells of permanent snow cover. Greenland was excluded from the analysis. There are indeed few products providing reliable snow cover information, due to the complex coastal topography and the difficulty of discriminating snow from ice (Brown *et al* 2010). Latitudes below 30°N were also excluded from the analysis because patchy snow or thin snow cover on vegetated surfaces may be missed in visible and near-infrared images (Riggs *et al* 2006). In order to explore the detailed information about changes in SCP over the NH, we analyzed changes in Eurasia (EU) and North America (NA) separately. Considering the fluctuation of SCE over the years, we confined our study area to stable snow-covered regions where snow covered the ground for at least 8 weeks (about 60 days) in 75% of the years between 1982 and 2013, following Choi *et al* (2010). The study area is displayed in figure 1.

In order to compare the SCP between different years, we used the hydrological year in this study. Based on the seasonal cycles of observed snow cover for northern EU and NA (Brutel-Vuilmet *et al* 2013), we defined the hydrological year of the NH as the period between September of a given year $(t-1)$ and August of the following in year (t). Moreover, we defined the accumulation season of snow cover as extending from September of a given year $(t-1)$ until the next February of the following year (t), while the melting season ranged from March to August of a same year (t). For the binary and weekly NHSCE dataset, we first identified the date range $(i–i+6)$ of the first frame (m) when the snow cover first appeared in the accumulation season, as well as the date range $(j–j+6)$ of the last frame (n) when the snow cover first disappeared in the melting season. Then, D_o and D_e of the year (t) were defined as the date $i+3$ of the frame (m) in the accumulation season and $j+3$ of the frame (n) in the melting season. D_d was defined as the time span between D_o and D_e.

2.2.2. Contribution analysis

Changes in the SCP over the NH are determined using the SCP anomalies over the EU and NA. To compare the contributions of SCP anomalies in EU and NA consistently, SCP variations over the NH, EU, and NA were converted into the standardized SCP anomalies (z-score) in the contribution analysis using the mean and the standard deviation of each series between 1982 and 2013. The contributions of EU and NA SCP anomalies to the NH SCP variability were computed annually to display the changing influence of EU and NA SCP anomalies on the underlying NH SCP variability.

The contributions of EU and NA SCP anomalies to the NH SCP variability were computed by regressing the annual series of NH SCP z-scores against the z-scores time series of the EU and NA SCP series. The resulting regression coefficients were then multiplied by the time series of EU and NA SCP z-scores to derive the contributions of the EU and NA SCP to the NH SCP variability. This method was employed by Pederson *et al* (2013) to identify regional patterns and

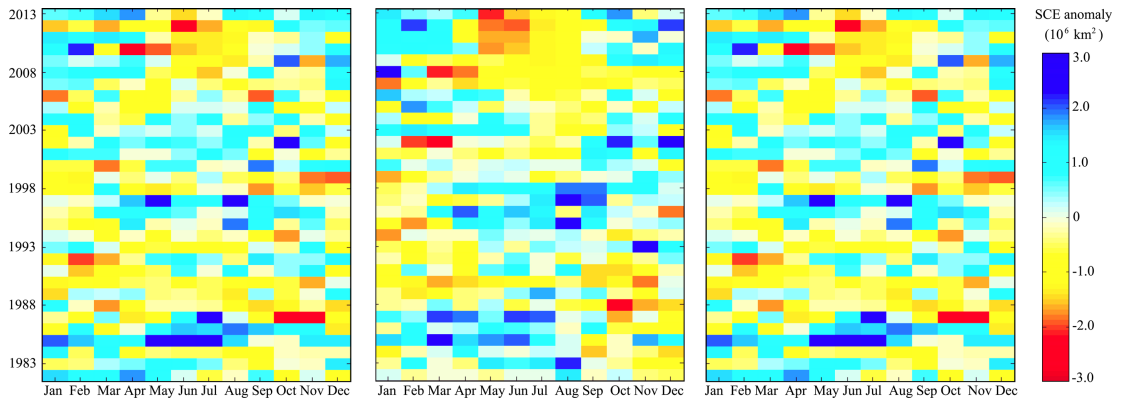

Figure 2. Monthly SCE anomaly over the Northern Hemisphere (left), Eurasia (middle), and North America (right) from 1982 to 2013. Chart data are from the Rutgers University Global Snow Lab (http://climate.rutgers.edu/snowcover/).

proximal causes of the recent snowpack decline in the Rocky Mountains.

2.2.3. Radiative forcing and feedback calculation

The radiative kernel method is widely used to quantify the radiative forcing induced by a_s changes. For example, Flanner *et al* (2011) quantified the radiative forcing from albedo change induced by changes in the NH cryosphere. Chen *et al* (2015) calculated the SCP change and its associated radiative cooling. In the present study, the albedo radiative kernels developed by Shell *et al* (2008) and Soden *et al* (2008) were used to quantify the S_nRF and the feedback caused by the albedo change, which is induced by the SCP anomaly. Compared with analytical models, the radiative kernel methods are more accurate because they capture more effectively the functional dependence of the planetary albedo upon the surface albedo (Qu and Hall 2014), which is one of the most important parameters in the quantification of the albedo-induced radiative forcing and feedback.

We defined the S_nRF as the instantaneous perturbation to Earth's TOA net SW anomalies consequent to the snow season variability. The a_s anomalies driven by the disappearance of snow cover during the melting season and by the presence of snow cover during the accumulation season allow to quantify this snow season variability. Thus, the time (t)-dependent S_nRF (W m^{-2}), within a region R (here, the NH snow-covered landmass) of an area A composed of grid cells r, can be represented as follows:

$$S_nRF(t,\ R) = \frac{1}{A(R)}\int_R S(t,\ r)\frac{\partial \alpha_s}{\partial S}(t,\ r)\frac{\partial F}{\partial \alpha_s} \times (t,\ r)\mathrm{d}A(r), \quad (1)$$

where S is the snow cover fraction (SCF) over the study area, $\partial\alpha_s/\partial S$ is the rate of variation of the surface albedo with the snow cover change, and $\partial F/\partial\alpha_s$ is the response of the TOA net SW anomalies to a_s change. We assumed that the monthly and spatially varying $\partial\alpha_s/\partial S$ and $\partial F/\partial\alpha_s$ are constant for the SCF S and the surface albedo α_s, respectively. Then, $\partial\alpha_s/\partial S$ can be replaced with the mean albedo contrast induced by the snow cover anomaly and $\partial F/\partial\alpha_s$ can be obtained from the albedo radiative kernels (Flanner *et al* 2011, Chen *et al* 2015).

The strength of the albedo feedback induced by changes in SCP can be quantified using the S_nRF/T_s values. In our study, S_nRF/T_s is defined as the amount of additional TOA net SW radiation averaged over the decreases in NH extra-tropical landmass a_s, in association with a 1 °C increase in surface air temperature (T_s) (Hall and Qu 2006, Qu and Hall 2007). We first calculated the S_nRF for each month, then obtained the annual-mean S_nRF by averaging monthly S_nRF values from September to August, as defined in section 2.2.1. Similarly, we obtained the mean S_nRF per accumulation season by averaging S_nRF values from September to February and the mean S_nRF per melting season by averaging S_nRF between March and August.

3. Analysis of the results

3.1. Observed changes in SCE

The monthly SCE anomalies over the NH between 1982 and 2013, including EU and NA, are shown in figure 2. Detailed changes of monthly SCE over the NH are presented in table 1. As shown in figure 2 and table 1, the May–June–July–August (MJJA) period experienced a significant SCE reduction (−0.89 10^6 km^2 decade^{-1}) at the 95% significance level, especially after the year 2008 (−2.55 10^6 km^2 decade^{-1}). However, the monthly SCE variability over the 1998–2008 period in MJJA presented substantially different temporal anomalies in EU and NA. EU experienced a continuous SCE reduction after 1998 (−0.75 10^6 km^2 decade^{-1}), contrasting with the SCE increase in NA (0.03 10^6 km^2 decade^{-1}).

In contrast with the marked MJJA SCE reduction, the SCE increased over November–December–January–February (0.65 10^6 km^2 decade^{-1}), especially after the year 2002. This temporal pattern in the accumulation season is consistent with the pattern of

Table 1. SCE changes (10^6 km^2) in each month over the Northern Hemisphere (NH), North America (NA), and Eurasia (EU), from 1982 to 2013.

	January	February	March	April	May	June	July	August	September	October	November	December
NH	**1.42**	1.50	−0.10	−0.96	**−2.99**	**−4.07**	**−1.47**	**−0.41**	−0.18	**4.01**	1.38	**2.07**
	(0.08)	(0.15)	(0.93)	(0.26)	(0.00)	(0.00)	(0.00)	(0.05)	(0.72)	(0.00)	(0.21)	(0.02)
NA	−0.06	0.47	0.16	−0.09	**−0.92**	**−1.52**	**−0.57**	**−0.07**	0.05	**0.80**	0.03	0.68
	(0.86)	(0.28)	(0.68)	(0.88)	(0.04)	(0.00)	(0.00)	(0.01)	(0.81)	(0.05)	(0.95)	(0.18)
EU	**1.49**	1.03	−0.26	−0.88	**−2.07**	**−2.54**	**−0.97**	**−0.44**	0.09	**3.19**	1.33	**1.39**
	(0.04)	(0.24)	(0.79)	(0.20)	(0.00)	(0.00)	(0.00)	(0.00)	(0.83)	(0.00)	(0.12)	(0.03)

Note. *P* values are shown in parentheses. Bold values indicate changes that are significant at the 95% level.

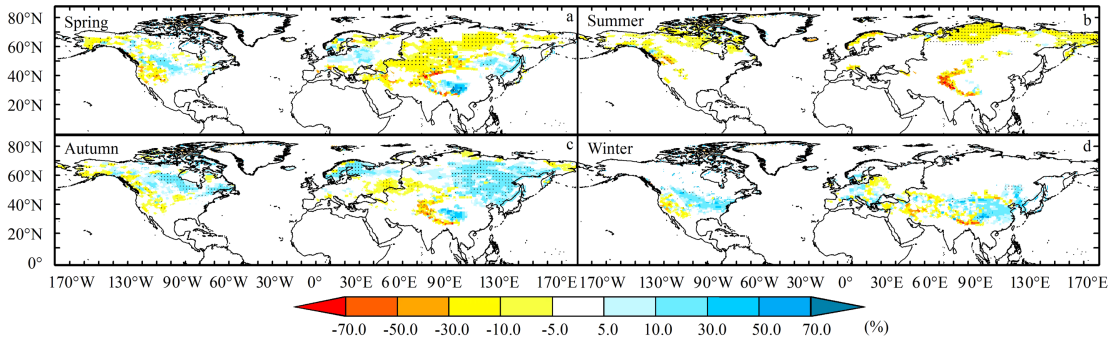

Figure 3. SCF changes over the Northern Hemisphere from 1982 to 2013 calculated from the NHSCE dataset for (a) spring (March–April–May), (b) summer (June–July–August), (c) autumn (September–October–November), and (d) winter (December–January–February). Black dots in (a)–(d) indicate that changes are statistically significant at the 95% level.

cooling in the winter, from 2002 to 2012 (Kosaka and Xie 2013). Kosaka and Xie (2013) found that T_s in the cold season (November–April) decreased over NH between 2002 and 2012, whereas global temperatures continued to rise.

Seasonal SCF anomalies were used to further investigate the spatial pattern of SCE anomalies over the NH from 1982 to 2013. For each pixel, the SCF was expressed as the percentage of snow cover appearance in a given season. The temporal anomalies of SCE over the NH were further verified by the spatial anomalies of SCF displayed in figure 3. The spring SCF in EU and Western NA, as well as the summer SCF over the entire NH, significantly decreased over the 1982–2013 period, during which there was a reduction of SCF in summer reaching up to 50% in high latitudes around 70°N at the 95% significance level. In contrast, the SCF in autumn and winter experienced a significant increase with magnitudes ranging 5%–30% at all latitudes over the NH. Increased SCF, especially in EU, extends the findings of Bulygina *et al* (2011) to a larger spatial scale, showing that the Russian territory has been experiencing an increase in snow depth since 1966, in the context of global temperature rise and sea ice reduction in the northern hemisphere. Moreover, the spatiotemporal distribution of SCF in autumn and winter coincides with the increasing snow cover and widespread boreal winter cooling observed over the last two decades (Cohen *et al* 2012).

3.2. Changes in SCP over the NH

The spatial distributions of annual mean D_o, D_e, and D_d, retrieved from NHSCE and averaged over the 1982–2013 period, and the contributions from EU and NA are shown in supplementary figure s1. The 32 year changes and the inter-annual variability in D_o, D_e, and D_d during the period of 1982–2013 are displayed in figure 4. Changes are estimated as the linear slope multiplied by the time interval in this study.

The 32 year averaged D_o displayed a mean value of day of year (DOY) of 301.13 over the NH stable snow-covered regions. The DOY values for EU and NA are 302.62 and 298.38, respectively (supplementary figure s1(a)). As displayed in figure 4(a), the 32 year changes in D_o presented high spatial heterogeneity across regions of the NH. In Eastern Asia, Eastern NA, and Western Europe, most of the pixels had an earlier D_o at the 95% significant level. The earlier D_o resulted in the increased autumn SCF, as displayed in figure 3(c). The inter-annual variability of D_o (figure 4(b)) revealed that the overall changes in D_o were relatively stable from 1982 to 2013 (no statistical significance). A contribution analysis demonstrated that the D_o anomalies in EU accounted for 78% of all D_o changes over the entire NH between 1982 and 2013 (figure 5(a)). The SCE changes in EU dominated D_o anomalies over the NH.

The 32 year averaged D_e displayed a mean DOY value of 132.66 over the NH stable snow-covered landmass. The values for EU and NA were 128.74 and 139.86, respectively (supplementary figure s1(c)). The 32 year changes in D_e over NH, EU, and NA were -6.12, -7.17 and -3.78 days decade^{-1} (no statistical significance), respectively. As shown in figure 4(c), almost all of the pixels over the NH snow-covered landmass, from low to high latitude, had an earlier D_e over the 1982–2013 period. However, the contribution analysis indicated that D_e changes in EU accounted for 73% of the D_e anomaly over the NH from 1982 to 2013, while D_e changes in NA only accounted for 27% of the NH D_e changes (figure 5(b)). This result extends the findings of Peng *et al* (2013) from the level of *in situ* observation to that of large continuous spatial coverage. Peng *et al* (2013) found, unlike their early D_e in EU (-2.6 ± 5.6 days decade^{-1}), that the trends in D_e over the NA (0.1 ± 5.8 days decade^{-1}) exhibited a fragmented spatial pattern from 1978 to 2006.

The combined spatial and temporal changes in D_o and D_e led to longer D_d in central NA, Western Europe, and Eastern Asia (figure 4(e)). The 32 year averaged D_d displayed a mean value of 196.53, 191.11, and 206.48 days over the NH, EU, and NA, with a shortening trend between 1982 and 2013 of 1.04, 1.17, and 1.33 days decade^{-1}, respectively. Although a statistical

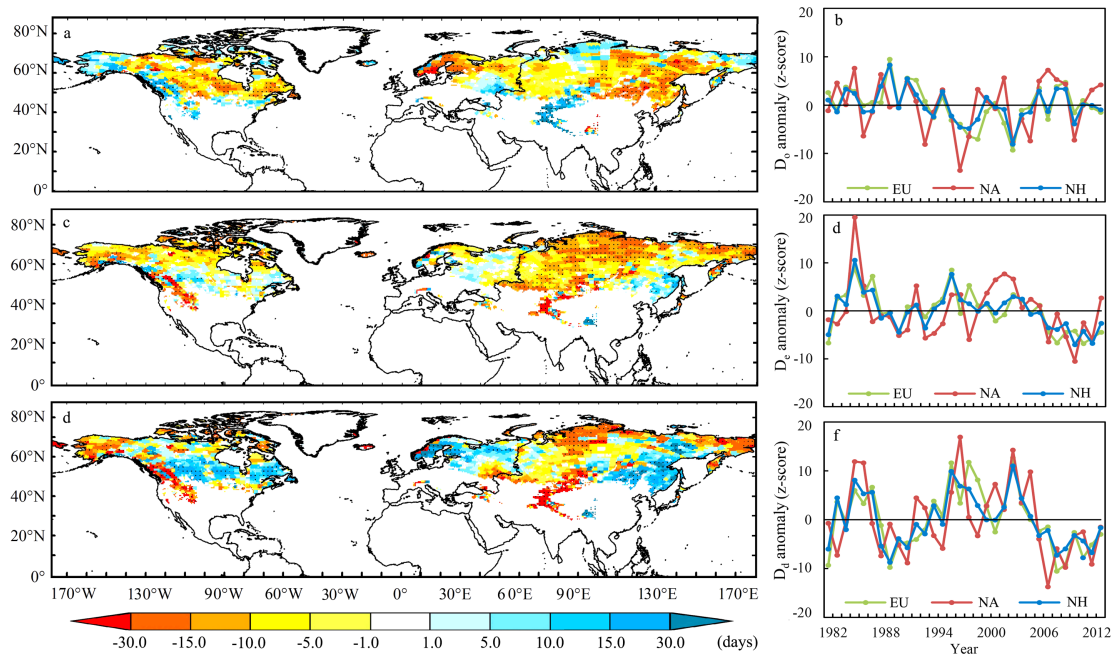

Figure 4. 32 year changes (days) of (a) D_o, (c) D_e, and (e) D_d over the Northern Hemisphere from 1982 to 2013. The inter-annual variability of (b) D_o, (d) D_e and (f) D_d between 1982 and 2013. The black dots in (a), (c), and (e) indicate changes that are significant at the 95% level. Negative changes in D_o, D_e, and D_d indicate earlier D_o, advanced D_e, and shorter D_d; positive changes in D_o, D_e, and D_d indicate later D_o, delayed D_e, and longer D_d over the NH from 1982 to 2013.

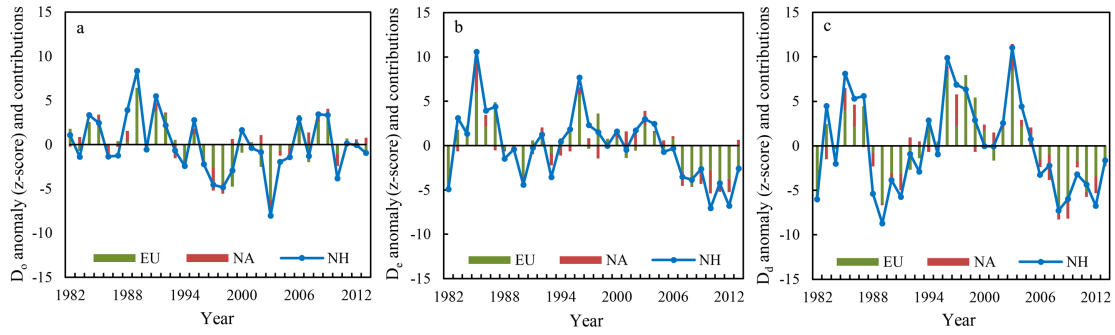

Figure 5. Interannual variations (days) in (a) D_o, (b) D_e, and (c) D_d over the NH from 1982 to 2013, and the corresponding contributions from EU and NA.

analysis based on the linear regression model revealed that there were no significant changes in D_d from 1982 to 2013, the inter-annual variability of D_d still presented a sharp shortening trend after the year 2006, which was caused by the delayed D_e over this period. These findings largely coincide with the significant reductions of SCE in May and June SCE in Derksen and Brown (2012). The high contributions from EU in the D_o and D_e anomalies result in a correspondingly high D_d anomaly in EU. The contribution analysis indicated that EU accounted for 76% of the D_d changes over the NH, against only 24% for NA over this period (figure 5(c)).

The correlation analysis of D_o, D_e, and D_d reveal significant relationships ($\geqslant$99%, Pearson correlation analysis) between D_e and D_d ($r = 0.78, 0.70, 0.79$ for the NH, EU, and NA, respectively) over the 1982–2013 period. The correlations between D_o and D_d ($r = 0.69$, 0.73, 0.63 for the NH, EU, and NA, respectively) are also significant at the 95% level. Considering that there are no statistically significant changes in D_o, the SCP changes over the NH from 1982 to 2013 are mostly attributed to the changes in D_e, as demonstrated by future snow cover changes in EU.

3.3. Changes in the snow radiative forcing S_nRF and the albedo feedback

The spatial distributions of annually averaged clear-sky S_nRF, accumulation season S_nRF_a and melting season S_nRF_m and their changes over the NH snow-covered landmass between 1982 and 2013 are shown in supplementary figure s2 and figure 6. We calculated the S_nRF per month, and averaged the monthly S_nRF values from the accumulation season and from the

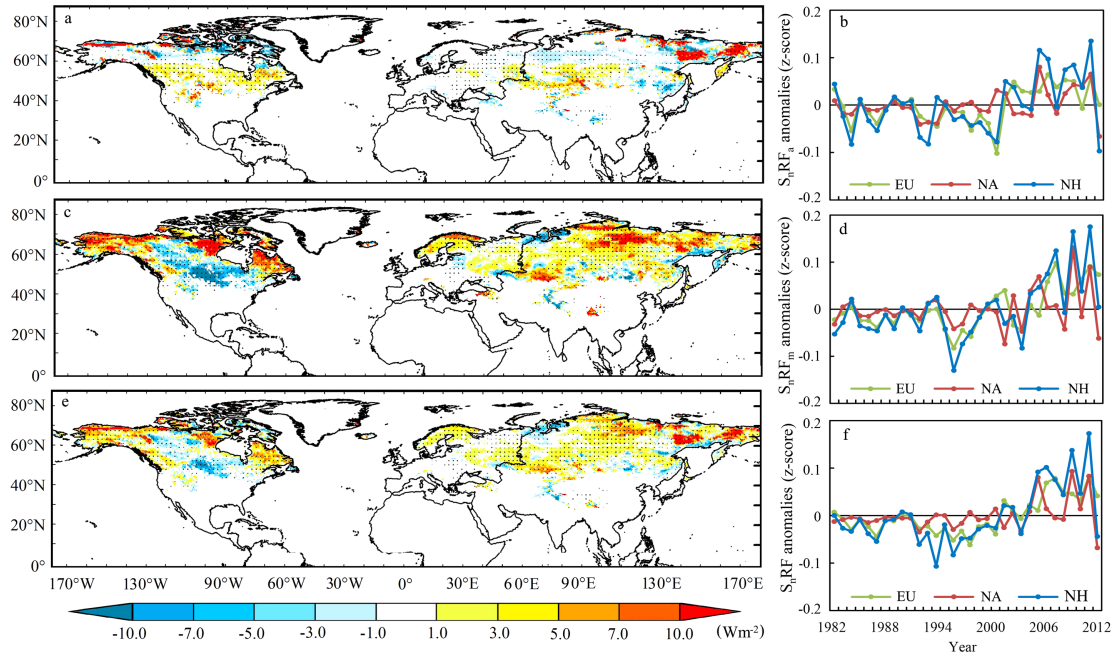

Figure 6. 32 year changes in (a) S_nRF_a, (c) S_nRF_m, and (e) S_nRF over the Northern Hemisphere from 1982 to 2013. Inter-annual variations of (b) S_nRF_a, (d) S_nRF_m, and (f) S_nRF over the NH from 1982 to 2013. The black dots in (a), (c), and (e) indicate changes that are significant at the 95% level.

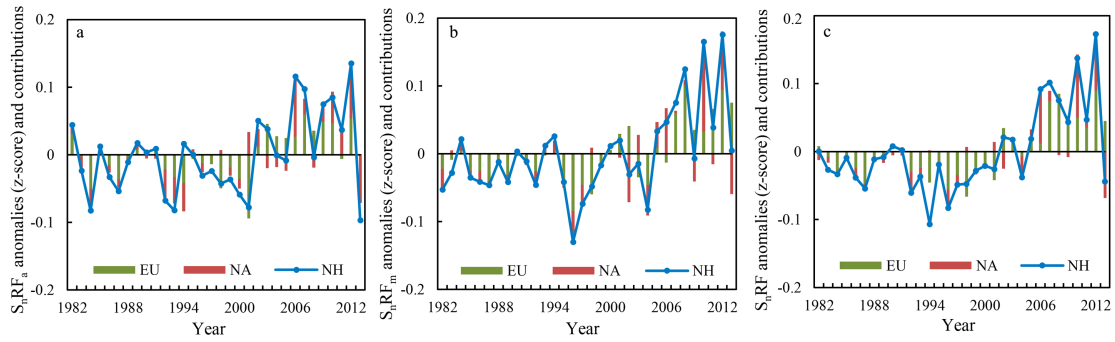

Figure 7. Inter-annual variability of (a) S_nRF_a, (b) S_nRF_m, and (c) S_nRF over the Northern Hemisphere from 1982 to 2013 and the corresponding contributions from Eurasia (EU) and North America (NA).

melting season to obtain the value of S_nRF_a and S_nRF_m, respectively. Determined by the spatial pattern of SCP anomalies and the magnitude of the albedo radiative kernels in the high-to-low latitudes, the S_nRF is generally larger over the high latitudes in the melting season (figure s2(b)), as well as in the entire snow season (figure s2(c). This is a consequence of the large Δa_s induced by a larger SCF compared with the low-to-mid latitudes, which shows a different distribution from the S_nRF in the accumulation season (figure s2(a)).

The spatial distribution of S_nRF_m changes (figure 6(c)) presents weakened cooling effects with smaller magnitude of S_nRF_m in high latitude landmass near the Arctic Ocean, and strengthened cooling effects with larger magnitude of S_nRF_m in the central United States from 1982 to 2013. This coincides with the observed spatiotemporal anomalies of D_e (figure 4(c)). However, the S_nRF_m changes in NA are not statistically significant, which may be caused by the contrast between S_nRF_m changes over the mid- and high latitudes in this region. The spatial distribution of S_nRF change is displayed in figure 6(e), which shows that longer D_d in the central United States resulted in a correspondingly strengthened S_nRF in this region. However, the longer D_d distributed over Europe and Eastern Asia does not match well the distribution of S_nRF in this region.

The 32 year interannual variations of clear-sky S_nRF_a, S_nRF_m, and S_nRF from 1982 to 2013 are shown in figures 6(b), (d) and (f). The 32 year changes in S_nRF_a, S_nRF_m, and S_nRF over the NH are 0.09 ($\pm$0.009), 0.12 ($\pm$0.003), and 0.10 ($\pm$0.005) W m^{-2}, respectively, at the 95% significant level. The statistical analysis revealed that EU accounted for 68%, 74%, and 70% of the changes in S_nRF_a, S_nRF_m, and S_nRF,

respectively, from 1982 to 2013 (figure 7). The estimated NH warming over the 1982–2013 period obtained from the Goddard Institute for Space Studies Surface Temperature Analysis (Hansen *et al* 2010) is 0.59 °C (from September 1981 to August 2013). The ranges of S_nRF_a, S_nRF_m, and S_nRF combined with this warming yield changes in the accumulation season, melting season and entire snow season albedo feedback (S_nRF/T_s) of 0.18 (±0.008), 0.21 (±0.005), and 0.17 (±0.008) W m^{-2} K^{-1}, respectively, over the NH.

4. Discussion and conclusion

SCP is one of the most sensitive factors to changes in climate. In this study, D_o, D_e, and D_d were retrieved, based on observed NHSCE snow cover data. The associated radiative forcing and feedback were quantified partly using the observed surface albedo dataset and the albedo radiative kernels technology.

Compared with the few changes in D_o, the 32 year anomalies in D_e over the NH displayed a marked trend of −1.91 days decade^{-1} at the 95% significance level. The contribution analysis indicated that the D_e change in EU (−2.24 days decade^{-1}) accounted for 73% of the D_e changes over the NH. The combined spatial and temporal changes in D_o and D_e led to a shortening trend of 1.04 days decade^{-1} over the NH from 1982 to 2013. However, earlier D_o still resulted in longer D_d in central NA, Western Europe, and Eastern Asia.

Driven by the SCP anomalies over the NH, the associated radiative forcing in the accumulation season, melting season, and entire snow season from 1982 to 2013 are 0.09 (±0.009), 0.12 (±0.003), and 0.10 (±0.005) W m^{-2}, respectively. Even through there are no statistically significant changes in D_o, the anomaly in accumulation season radiative forcing is still significant at the 95% level. The statistical analysis revealed that EU accounts for 68%, 74%, and 70% of the changes in S_nRF_a, S_nRF_m, and S_nRF over the NH between 1982 and 2013, which is consistent with the high contributions from EU to the SCP changes. However, S_nRF_m changes in NA are not statistically significant, due to the contrasting S_nRF_m changes in the mid- and high latitudes induced by the distribution of D_e anomalies in this region.

Compared with previous research, the present study investigated the SCP changes, quantified the associated radiative forcing and feedback, and explored the contributions from EU and NA, which is important for current climate change studies and future climate projections. However, several unresolved issues remain in our study. S_nRF is influenced by several factors, including the a_s change induced by snow, the local insolation, and the atmospheric state (Flanner *et al* 2011). Limited by the spatial resolution of NHSCE snow cover dataset, the snow range used in this study includes variability caused by both unresolved snow cover variability and variability in the influence of vegetation on albedo contrast. Considering the rapid responses of the permafrost and vegetation to experimentally increased snow cover (Johansson *et al* 2013), a separation of vegetation effects from S_nRF quantification is necessary in future studies. In addition, since the NH warming trend is very likely to continue due to increasing greenhouse gas concentrations and intensified Arctic amplification effects, the SCP is also likely to experience rapid changes in the near future, which should be a high concern in climate change projections.

Acknowledgments

The snow cover data used in this study were provided by the National Snow and Ice Data Center and the Rutgers University Global Snow Lab. The GLASS albedo products were provided by Beijing Normal University. This study was partially funded by the High-Tech Research and Development Program of China under grant 2013AA121201 (SL), the Joint Polar-Orbiting Satellite System Program (SL), and Chinese Scholarship Council (XC and YC).

References

Barnett T, Adam J and Lettenmaier D 2005 Potential impacts of a warming climate on water availability in snow-dominated regions *Nature* **438** 303–9

Bokhorst S, Bjerke J, Tømmervik H, Callaghan T and Phoenix G 2009 Winter warming events damage sub-Arctic vegetation: consistent evidence from an experimental manipulation and a natural event *J. Ecol.* **97** 1408–15

Brands S 2014 Predicting average wintertime wind and wave conditions in the North Atlantic sector from Eurasian snow cover in October *Environ. Res. Lett.* **9** 045006

Brown R, Derksen C and Wang L 2010 A multi-data set analysis of variability and change in Arctic spring snow cover extent, 1967–2008 *J. Geophys. Res.* **115** D16111

Brown R and Robinson D 2011 Northern Hemisphere spring snow cover variability and change over 1922–2010 including an assessment of uncertainty *Cryosphere* **5** 219–29

Brutel-Vuilmet C, Ménégoz M and Krinner G 2013 An analysis of present and future seasonal Northern Hemisphere land snow cover simulated by CMIP5 coupled climate models *Cryosphere* **7** 67–80

Bulygina O, Groisman P, Razuvaev V and Korshunova N 2011 Changes in snow cover characteristics over Northern Eurasia since 1966 *Environ. Res. Lett.* **6** 045204

Chen X, Liang S, Cao Y and He T 2016 Distribution, attribution, and radiative forcing of snow cover changes over China from 1982 to 2013 *Clim. Change* **137** 363–77

Chen X, Liang S, Cao Y, He T and Wang D 2015 Observed contrast changes in snow cover phenology in northern middle and high latitudes from 2001–2014 *Sci. Rep.* **5** 16820

Choi G, Robinson D and Kang S 2010 Changing Northern Hemisphere snow seasons *J. Clim.* **23** 5305–10

Cohen J, Furtado J, Barlow M, Alexeev V and Cherry J 2012 Arctic warming, increasing snow cover and widespread boreal winter cooling *Environ. Res. Lett.* **7** 014007

Derksen C and Brown R 2012 Spring snow cover extent reductions in the 2008–2012 period exceeding climate model projections *Geophys. Res. Lett.* **39** L19504

Flanner M, Shell K, Barlage M, Perovich D and Tschudi M 2011 Radiative forcing and albedo feedback from the Northern Hemisphere cryosphere between 1979 and 2008 *Nat. Geosci.* **4** 151–5

Frei A, Tedesco M, Lee S, Foster J, Hall D, Kelly R and Robinson D 2012 A review of global satellite-derived snow products *Adv. Space Res.* **50** 1007–29

Gouttevin I, Menegoz M, Dominé F, Krinner G, Koven C, Ciais P, Tarnocai C and Boike J 2012 How the insulating properties of snow affect soil carbon distribution in the continental pan-Arctic area *J. Geophys. Res. Biogeosci.* **117** G02020

Hall A 2004 The role of surface albedo feedback in climate *J. Clim.* **17** 1550–68

Hall A and Qu X 2006 Using the current seasonal cycle to constrain snow albedo feedback in future climate change *Geophys. Res. Lett.* **33** L03502

Hansen J, Ruedy R, Sato M and Lo K 2010 Global surface temperature change *Rev. Geophys.* **48** RG4004

He T, Liang S, Yu Y, Wang D, Gao F and Liu Q 2013 Greenland surface albedo changes in July 1981–2012 from satellite observations *Environ. Res. Lett.* **8** 044043

Helfrich S, McNamara D, Ramsay B, Baldwin T and Kasheta T 2007 Enhancements to, and forthcoming developments in the Interactive Multisensor Snow and Ice Mapping System (IMS) *Hydrol. Process.* **21** 1576–86

IPCC 2013 *Climate Change 2013: The Physical Science Basis. Contribution of Working Group I to the Fifth Assessment Report of the Intergovernmental Panel on Climate Change* ed T Stocker *et al* (Cambridge: Cambridge University Press)

Johansson M, Callaghan T, Bosiö J, Åkerman H, Jackowicz-Korczynski M and Christensen T 2013 Rapid responses of permafrost and vegetation to experimentally increased snow cover in sub-arctic Sweden *Environ. Res. Lett.* **8** 035025

Kosaka Y and Xie S 2013 Recent global-warming hiatus tied to equatorial Pacific surface cooling *Nature* **501** 403–7

Liang S *et al* 2013 A long-term Global LAnd Surface Satellite (GLASS) data-set for environmental studies *Int. J. Digital Earth* **6** 5–33

Moody E, King M, Schaaf C and Platnick S 2008 MODIS-derived spatially complete surface albedo products: spatial and temporal pixel distribution and zonal averages *J. Appl. Meteorol. Climatol.* **47** 2879–94

Pederson G, Betancourt J and McCabe G 2013 Regional patterns and proximal causes of the recent snowpack decline in the Rocky Mountains, US *Geophys. Res. Lett.* **40** 1811–6

Peng S, Piao S, Ciais P, Friedlingstein P, Zhou L and Wang T 2013 Change in snow phenology and its potential feedback to temperature in the Northern Hemisphere over the last three decades *Environ. Res. Lett.* **8** 014008

Qu X and Hall A 2006 Assessing snow albedo feedback in simulated climate change *J. Clim.* **19** 2617–30

Qu X and Hall A 2007 What controls the strength of snow-albedo feedback *J. Clim.* **20** 3971–81

Qu X and Hall A 2014 On the persistent spread in snow-albedo feedback *Clim. Dyn.* **4** 269–81

Riggs G, Hall D and Salomonson V 2006 MODIS Snow Products User Guide Collection 5 (https://nsidc.org/data/docs/daac/modis_v5/dorothy_snow_doc.pdf)

Robinson D, Dewey K, Richard R and Heim J 1993 Global snow cover monitoring: an update *Bull. Am. Meteorol. Soc.* **74** 1689–96

Shell K, Kiehl J and Shields C 2008 Using the radiative kernel technique to calculate climate feedbacks in NCAR's community atmospheric model *J. Clim.* **21** 2269–82

Soden B, Held I, Colman R, Shell K, Kiehl J and Shields C 2008 Quantifying climate feedbacks using radiative kernels *J. Clim.* **21** 3504–20

Wang L, Derksen C, Brown R and Markus T 2013 Recent changes in pan-Arctic melt onset from satellite passive microwave measurements *Geophys. Res. Lett.* **40** 522–8

Wegmann M *et al* 2015 Arctic moisture source for Eurasian snow cover variations in autumn *Environ. Res. Lett.* **10** 054015

Whetton R, Haylock M and Galloway R 1996 Climate change and snow-cover duration in the Australian Alps *Clim. Change* **32** 447–79